Electronic Supplementary Material (ESI) for RSC Advances.
This journal is © The Royal Society of Chemistry 2015

Supplementary Electronic Information (ESI)

Surface-Active Organic Matter induces salt morphology transitions during new atmospheric particle formation and growth

Vangelis Daskalakis[1]*, Fevronia Charalambous[1], Constantinos Demetriou[1] and Georgia Georgiou[1]

[1]Cyprus University of Technology, Department of Environmental Science and Technology, P.O. Box 50329, 3603 Limassol – Cyprus.

***Corresponding Author:** Vangelis Daskalakis

Tel: +357 25002458, Fax. +357 25002820. E-mail: evangelos.daskalakis@cut.ac.cy

Contents

1. Equilibration/ Relaxation Protocol

The equilibration/ relaxation runs for the models were performed using the Desmond 2014.2 Molecular Dynamics (MD) package.[1] In detail, Brownian Dynamics at 10K for 200ps were employed along with two short 24ps runs in NVT and NpT ensembles at 10K with the weak-coupling Berendsen thermostat-barostat.[2]

Desmond MD package employs Brownian integrators that are based on the Langevin constant volume and temperature dynamics in the limit as $\tau=\tau_b \rightarrow 0$. The equations of motion proceed as modified NVT dynamics to stabilize the equilibration process from starting points with very large potential energies or forces. In this consensus, any inertial information is lost. All velocities are *clipped*, enforcing also a maximum displacement of a 0.01nm length for all particles, in any direction on every position update. This becomes superfluous later and avoids runaway particles, or a collapsing, exploding simulation cell (*see Desmond Manual*).[3]

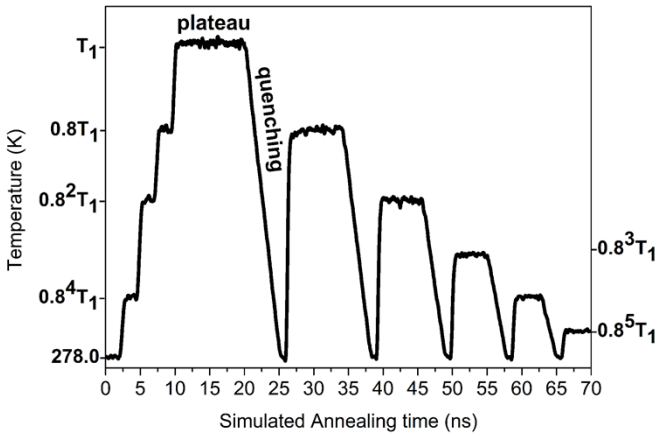

Figure S1. The "sawtooth" Simulating Annealing (SA) cycles, depicting plateau and quenching parts.

2. Sampling through Simulated Annealing

An increase of the temperature of the equilibrated samples was performed in a Simulated Annealing (SA) ensemble at constant density from 10.0K to 278.0K at a 100ps transition step and equilibration over a period of 400ps (278.0K) with the Nosé-Hoover thermostat[1, 4, 5] and T coupling constant of 1.0ps. A NpT ensemble run with the Martyna-Tobias-Klein (MTK) barostat coupled to the Nosé-Hoover thermostat,[4-6] followed at 278.0K for 4.0ns. T-P coupling constants of 1.0 and 2.0ps were used, respectively. In order to destruct any setup based biased salt morphology, each sample was heated at a considerably large temperature T_1 till evaporation in an adapted constant density Molecular Dynamics (MD) SA run based on Kirkpatrick et al.[7] and

the "sawtooth" method by Topper et al.[8] for the adequate conformational sampling. This protocol has been successfully used to probe the dynamics of ammonium chloride salts elsewhere.[8] A "sawtooth" cycle is shown in **Figure S1**. T_1 must be sufficiently high for ergodic sampling in the simulation time scale. For this we increase the temperature of each sample from 278.0K to T_1 gradually with 500ps transition steps and equilibrate for 2.0ns at each intermediate temperature of 0.8^4T_1, 0.8^2T_1 and $0.8T_1$. At T_1 the samples equilibrate for 10.0ns (plateau time t_1), then the temperature drops to 278.0K over a period of 5.0ns (quenching time t_2) and equilibrate at 278.0K for 1.0ns. The samples are then subjected to sharp (100.0ps step) increases in the temperature between 278.0K and $0.8T_1$, 0.8^2T_1, 0.8^3T_1, 0.8^4T_1 and 0.8^5T_1 with respective plateau times of $0.8t_1$, 0.8^2t_1 etc. and quenching times of $0.8t_2$, 0.8^2t_2 etc. back to 278.0K and a 1.0ns equilibration at 278.0K. After the 70.0ns "sawtooth" cycle, a temperature decrease under constant pressure (MTK at 1.0atm) from 0.8^5T_1 to 278.0K (2.0ns) and equilibration for another 2.0ns at 278.0K follows. Due to the large number of possible minima for the molecular clusters, the configuration space has to be sampled adequately to ensure global minima. Four input structures per sample for the following production simulations were generated, thus, as the final conformations out of the previous "sawtooth" cycles with the four (4) different high T_1values of 900.0, 1020.0, 1120.0 and 1220.0K. High T_1 values evaporate the samples at short simulation times, while the harmonic potential used ensures no molecular bond breakage. T_1 is above both the melting and boiling temperatures of NH_4Cl (611, 793K) and it induces efficient mixing of the aerosol contents in the relaxation-equilibration time used (70.0ns).

3. Production Simulations – Single Nucleus Systems

Production simulations for all systems in **Table 1** (*see main manuscript*) consist of (a) constant density and temperature (NVT, 278.0K) runs with the Nosé-Hoover thermostat[4, 5] and T coupling constant of 1.0ps for 100.0ns to simulate the spherical morphology of a sole nucleus in the ambient environment, and (b) NpT constant pressure (1.0atm) and temperature (278.0K) runs with a fully flexible simulation cell and the Martyna-Tobias-Klein (MTK) barostat[6] coupled to the Nosé-Hoover thermostat[4, 5] and T-P coupling constants of 1.0 and 2.0ps, respectively, for 100.0ns to describe the bulk nucleus morphology. Four production trajectories were run per each sample/ ensemble for statistical analysis. Selected systems were probed for longer times (up to 300ns), but potential energies, volumes (for the NpT runs) and final geometries do not

change significantly by the smaller production simulation end times. The TIP4P-EW water potential freezes at much lower temperatures,[9] so the ice nucleation process does not interfere with particle morphologies.

4. Production Simulations – Large (two) Nuclei Systems

Pairs of $[(NH_4^+Cl^-)_{128}(OM)_y(H_2O)_{250}]$ nuclei (y=0, 30, or 80) with the salts restrained at the positions of all the variant salt morphologies identified at the end of the previous 100.0ns production trajectories produce cubic simulation cells with sides of 15.5 or 21.0nm dependent on the distance between the two nuclei (4.5 or 9.0nm), while the volume occupied by the molecules, including native and added water, varied between 80-110 nm^3 or 130-160 nm^3, dependent on the separating distance and the individual nuclei sizes. The added water content to the two $[(NH_4^+Cl^-)_{128}(OM)_y(H_2O)_{250}]$ nuclei is at around 1000, or 2400 molecules for the 4.5, or 9.0nm separation distances, respectively. Production runs are based on the aforementioned production NVT methodology for the pairs and it is employed for 11.0ns at 278K. No significant changes in the density, potential energies or actual structures were observed past this time.

5. The Radial Distribution Function (RDF)

There exist several elaborate methods in the literature to identify and quantify clusters in Molecular Dynamics Simulations, but an extensive use of quantitative cluster identification criteria and the comparison between different techniques [10-16] exceed the scope of this work. On the other hand, the radial distribution functions (RDFs) consist the most straightforward way to quantify the degree of ion pairing in a crystal.[17] They provide useful information on the local structure in a globally homogeneous system with the time averages being directly associated with cluster structures, order or disorder, shapes, sizes and stability over time. We chose to probe the NH_4Cl clusters using the RDF method in this study. In addition, the RDF approach proves also suitable to identify a potential concentration of OM on the surface of a forming particle.[18]

To identify (and quantify) the different salt morphologies, we calculate the N-N pair RDF for each sample. Averaging is used out of the production trajectories in a way that large standard error bars indicate that the production trajectories yield both crystalline and disordered salt morphologies; whereas smaller error bars indicate that the salt within the sample transitions mainly to the one or the other morphology. The highest

percentage of crystalline salt would be accompanied by an increase in the average $RDF_{N\text{-}N}$ intensity of a sample, as well as by the presence of sharp peaks and a large ratio of the first/second peak intensities. On the other hand, lower intensity average $RDF_{N\text{-}N}$ and lower ratio of the first/second peak intensities indicate that more trajectories lead to the disordered salt morphology that consists a highly concentrated aquatic salt solution (brine). All RDF profiles in this study have been calculated at 0.20Å resolution. This was the lowest resolution to avoid noise and produce converged plots that do not change significantly by changing slightly the resolution.

6. Calculation of the Static Dielectric Constant ε of water solvent

We calculated the static dielectric constant at the conditions reported in the NVT production runs. The ε values over time may be obtained from the fluctuations of the total dipole moment M for all the TIP4P-EW water molecules using the equation $\varepsilon = 1 + \frac{\langle M^2 \rangle - \langle M \rangle^2}{3\varepsilon_0 V K_B T}$ for a non-polarizable water potential.[19] The angled brackets represent ensemble averages, ε_0 is the vacuum permittivity, V is the volume of the system, K_B is the Boltzmann-constant and T is the temperature. Four production trajectories of 100ns each were used for each system of the formulas $[(NH_4Cl)_{89}(OM)_{80}(H_2O)_{500}]$, $[(NH_4Cl)_{96}(OM)_{80}(H_2O)_{500}]$, $[(NH_4Cl)_{89}(H_2O)_{500}]$ and $[(NH_4Cl)_{96}(H_2O)_{500}]$ in the NVT ensemble to calculate a time evolution of the ε values of the water solvent in each system. The time series of the total dipole moment M was calculated employing the Dipole Watcher plugin of the VMD 1.9.2 Software.[20] The ε time series are averaged over the four production trajectories per sample.

7. The radius of Gyration (R_g)

The Radius of Gyration (R_g) is calculated as the root mean square distance of the water oxygen atoms from the center of mass of the water accumulation, located roughly at the center between the large (two-nuclei) systems. The Rg is calculated as averages over the different trajectories of total simulation time at 44ns (uncontaminated samples) or 88ns (surface-active contaminated samples) for both methylglyoxal and

acetaldehyde contaminated nuclei. Fitting the Rg curves to the $Rg = base + \frac{Rg_{\max}}{\left[1 + ve^{-k(t-tm)}\right]^{1/v}}$ equation,

which is the asymmetrical sigmoidal growth function yields the Relative Growth Rates (RGR) as $k/(1+v)$. At the time tm the absolute growth rate reaches its maximum value.

8. The Absolute Solvation Free Energies (ASFE)

Dry salt clusters are isolated at the end of the 100.0ns production trajectories by eliminating all TIP4P-EW waters and surface-active OM in all morphologies, so that only NH_4Cl species are left in the simulation cell. The same salt morphologies are identified in the NVT or NpT runs, but the NpT production runs were selected as they gave a large number of different salt morphologies at the same salt/water ratio (especially for the 128-NH_4Cl models). The dry (and OM-free) salts from the NpT runs, thus, were used as input structures for the calculation of the ASFE. The isolated (dry) neutral salts were re-solvated in orthorhombic water boxes using at least a 1.0nm buffer distance between salt atoms and the simulation cell sides and no additional ions. Buffers of 0.5nm and 0.7nm were also tested but the change in solvation energies ($\Delta\Delta G$) was negligible falling into the standard deviation (stdev) error. Explicit SPC waters were used for the solvation and the OPLS-2005 Force Field (FF) for the salts. There is a negligible difference in the output energies if TIP3P and TIP4P water models are used instead.[21] The MD simulation workflow for the Free Energy Perturbation (FEP) calculations was based on a "pseudo" double annihilation and the default Desmond protocol described in detail elsewhere. [21, 22] The 12-window λ schedule was implemented with 2.0ns of production simulation at each λ to predict the absolute solvation free energies (ASFE) for each model. This was performed by the Free Energy Perturbation (FEP) module implemented in the Desmond Molecular Dynamics (MD) program[1] for the different dry salt conformations/ morphologies identified in this study.

References

1. K. J. Bowers, E. Chow, H. Xu, R. O. Dror, M. P. Eastwood, B. Gregersen, J. L. Klepeis, I. Kolossvary, M. Moraes and F. D. Sacerdoti, Scalable algorithms for molecular dynamics simulations on commodity clusters, Proceedings of the 2006 ACM/IEEE conference on Supercomputing, Tampa, Florida, 2006.
2. H. J. Berendsen, J. P. M. Postma, W. F. van Gunsteren, A. DiNola and J. Haak, *The Journal of chemical physics*, 1984, **81**, 3684-3690.
3. D. E. Shaw-Research, *Desmond Users Guide Release 3.4.0/ 0.7.2*, 2013.
4. S. Nosé, *The Journal of chemical physics*, 1984, **81**, 511-519.
5. W. G. Hoover, *Physical Review A*, 1985, **31**, 1695-1997.
6. G. J. Martyna, D. J. Tobias and M. L. Klein, *The Journal of Chemical Physics*, 1994, **101**, 4177-4189.
7. S. Kirkpatrick, C. D. Gelatt and M. P. Vecchi, *science*, 1983, **220**, 671-680.
8. R. Q. Topper, W. V. Feldmann, I. M. Markus, D. Bergin and P. R. Sweeney, *The Journal of Physical Chemistry A*, 2011, **115**, 10423-10432.
9. H. W. Horn, W. C. Swope, J. W. Pitera, J. D. Madura, T. J. Dick, G. L. Hura and T. Head-Gordon, *The Journal of chemical physics*, 2004, **120**, 9665-9678.
10. F. H. Stillinger Jr, *The Journal of Chemical Physics*, 1963, **38**, 1486-1494.
11. Y. Chiew, G. Stell and E. Glandt, *The Journal of chemical physics*, 1985, **83**, 761-767.
12. J. Wedekind and D. Reguera, *The Journal of chemical physics*, 2007, **127**, 154516.
13. L. A. Pugnaloni and F. Vericat, *The Journal of chemical physics*, 2002, **116**, 1097-1108.
14. P. R. ten Wolde and D. Frenkel, *The Journal of chemical physics*, 1998, **109**, 9901-9918.
15. J. Wedekind, R. Strey and D. Reguera, *The Journal of chemical physics*, 2007, **126**, 134103.
16. B. Senger, P. Schaaf, D. Corti, R. Bowles, D. Pointu, J.-C. Voegel and H. Reiss, *The Journal of chemical physics*, 1999, **110**, 6438-6450.
17. J. Heyda, M. Lund, M. Oncak, P. Slavicek and P. Jungwirth, *The Journal of Physical Chemistry B*, 2010, **114**, 10843-10852.
18. V. Daskalakis, F. Charalambous, F. Panagiotou and I. Nearchou, *Physical Chemistry Chemical Physics*, 2014, **16**, 23723-23734.
19. O. Gereben and L. Pusztai, *Chemical Physics Letters*, 2011, **507**, 80-83.
20. W. Humphrey, A. Dalke and K. Schulten, *Journal of molecular graphics*, 1996, **14**, 33-38.
21. D. Shivakumar, J. Williams, Y. Wu, W. Damm, J. Shelley and W. Sherman, *Journal of Chemical Theory and Computation*, 2010, **6**, 1509-1519.
22. D. Shivakumar, E. Harder, W. Damm, R. A. Friesner and W. Sherman, *Journal of Chemical Theory and Computation*, 2012, **8**, 2553-2558.